ELSEVIER

Ultramicroscopy 66 (1996) 59–71

ultramicroscopy

Fresnel contrast analysis of composition changes and space charge at grain boundaries in mullite

Ferhat Kara[1], Rafal E. Dunin-Borkowski*, Christopher B. Boothroyd, John A. Little, W. Michael Stobbs[2]

Department of Materials Science and Metallurgy, University of Cambridge, Pembroke Street, Cambridge CB2 3QZ, UK

Received 1 July 1996; accepted 27 September 1996

Abstract

Grain boundaries in two mullite specimens have been characterised using Fresnel contrast analysis in the transmission electron microscope. A ratio of the scattering potential differences ΔV between the grains and the grain boundaries in the two specimens was obtained without needing to know the absolute specimen thicknesses of the regions examined. The characterisation of a glassy intergranular film in one specimen using energy dispersive X-ray spectroscopy then allowed the magnitude of ΔV at a crystalline boundary in the second specimen to be determined. For the first time, this scattering potential difference was interpreted in terms of contributions to the contrast from space-charge layers as well as changes in electron scattering factor and density.

Keywords: Fresnel contrast; Mullite; Grain boundaries; Space charge

1. Introduction

The presence of glass at grain boundaries is known to play an important role in the high-temperature mechanical properties of many ceramics. The transmission electron microscopy (TEM)-based analytical technique of Fresnel contrast analysis [1–3] is well suited to the characterisation of such boundaries. The technique involves the determination of variations in the average Coulomb electrostatic potential V_0 by the comparison of the Fresnel fringe profile characteristics in a through-focal series of images of an edge-on boundary with computer simulations. However, the unique interpretation of experimental Fresnel contrast data requires all of the possible contributions to a measured change in specimen potential to be considered.

Our aim here is to demonstrate, through a comparison of the Fresnel characterisation of grain boundaries in two mullite ($3Al_2O_3 \cdot 2SiO_2$) specimens, that the method can be used to assess

* Corresponding author.

[1] Present address: Seramik Müh. Andalou University, Yunusemre Kampusu, 26470 Eskisehir, Turkey.

[2] Deceased 26.4.1996.

PII S0304-3991(96)00078-2

possible contributions to the boundary contrast from space-charge layers as well as from changes in electron scattering factor and density.

2. Details of specimens examined

The two mullite specimens examined were prepared by a sol-gel process and had starting compositions within and close to the solid solution range of mullite, which lies between 58.5 and 62.6 mol% (70.5 and 74 wt%) Al_2O_3 for typical sintering temperatures of 1600–1650°C. Pseudoboehmite (surface area 170 $m^2 g^{-1}$, Baco Cerasol, BA Chemicals, Bucks, UK), dispersed in water at a pH of 3.4, and fumed silica (surface area 360 $m^2 g^{-1}$, No. S-S005, Sigma, St. Louis, MO), dispersed in water at a pH of 7, were mixed together vigorously for 0.5 h, and then gelled and dried at 80°C for 48 h. The specimens were sintered at 1600°C for 2 h, either in the gel form[3] or as pressed pellets. Mechanically polished fragments were prepared for TEM examination by Ar-ion milling and subsequent coating with carbon to prevent charging in the microscope. Specimens A and B had nominal compositions of 60.6 mol% (72.3 wt%) Al_2O_3 (close to the stoichiometric composition) and 63.1 mol% (74.4 wt%) Al_2O_3 (close to the Al_2O_3 end of the solid solution range of mullite) respectively, as confirmed by electron probe microanalysis. A preliminary examination of both specimens in the TEM showed extended three-grain junctions in specimen A, which contained amorphous material (diffuse dark field contrast, with the objective aperture at the position of an amorphous halo, extended smoothly along both the three-grain junctions and the grain boundaries), while the three-grain junctions and grain boundaries in specimen B typically exhibited no amorphous contrast and lattice fringe continuity across them in high-resolution images taken on a JEOL 4000EX II microscope [4]. For each of the experiments described below, care was taken to ensure that a "representative" boundary in the above sense was always examined for each specimen.

[3] Ceramic balls were used for milling the crushed gel. Although the ceramic balls are potentially a source of contamination, no differences in microstructure were observed between specimens of the same starting composition, as milled, and as sintered in the gel form.

3. Fresnel contrast data

The application of Fresnel contrast analysis to the characterisation of grain boundaries in the mullite specimens A and B is facilitated by the fact that the compositions and hence the values of V_0 within the *grains* are almost identical. At the same specimen thickness and defocus, a relative comparison of the magnitude of the fringe contrast in the two specimens, which is to first order proportional to the scattering potential difference ΔV between the grains and the boundaries, will therefore provide a ratio of the values of ΔV without the need for a knowledge of the specimen thicknesses examined. Inelastic scattering contributions to the contrast will also be similar and can be neglected to first order.

Through-focal series of edge-on boundaries in specimens A and B were taken at 120 kV using a Philips 400ST microscope ($C_s = 2.8$ mm), at a calibrated magnification of 118.7 k. The defocus step between images was 110 nm and the objective aperture used had a semi-angle of 5.7 mrad. (Airy disc radius 0.36 nm). For each series, the mullite grains were tilted to weakly diffracting orientations, and the tilt of the grain boundaries with respect to the electron beam was refined by using the symmetry of the Fresnel contrast. The values of beam convergence (typically about 0.5 mrad.) were similar, and the magnitude of specimen drift over the duration of each series was low. No evidence was found for preferential thinning of the boundaries at their intersection with the specimen edge. The width of the contrast in the image series analysed did not change with specimen thickness, indicating the projection of layers of constant width through the foil thickness.

Fig. 1 shows examples of experimental images of grain boundaries in specimens A and B. Qualitatively, the boundaries exhibited a bright central fringe underfocus and a dark fringe overfocus, which indicates that they have lower scattering potentials than the surrounding grains. For

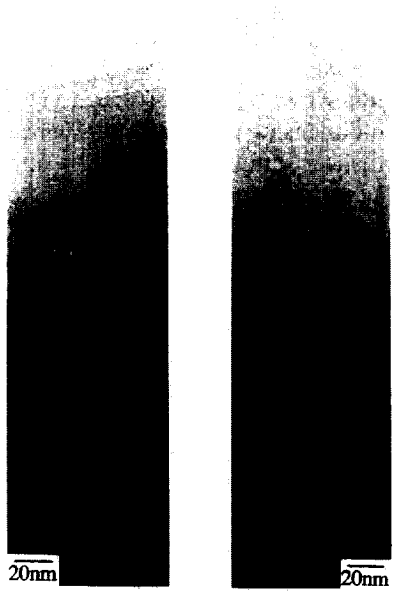

Fig. 1. TEM images taken from through-focal series of specimens A and B, at the defocus values indicated. The positions of the regions which were extracted digitally for analysis, and which correspond to intensities of 0.7, 0.6 and 0.55 relative to the value of 1 at zero crystal thickness in each specimen, are marked using the symbols 1, 2 and 3, respectively.

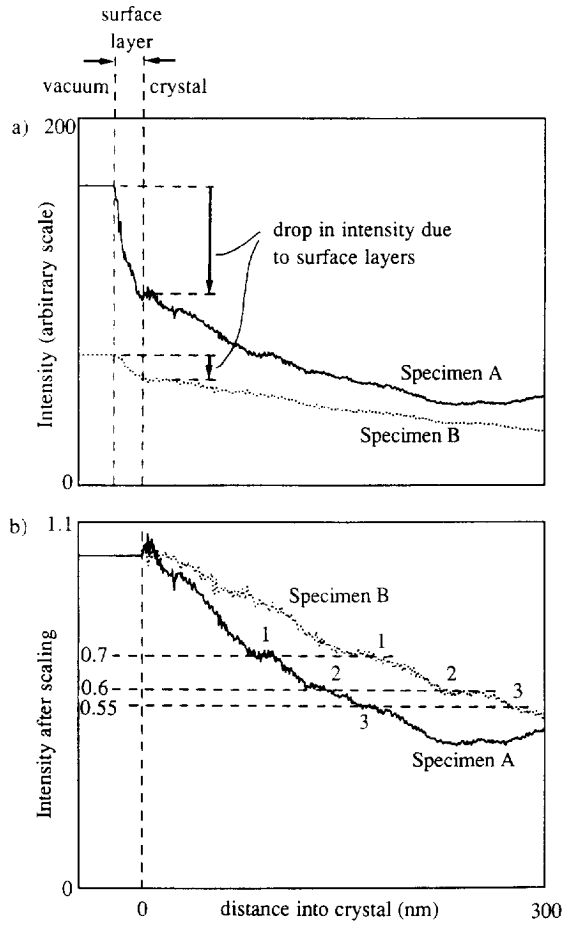

Fig. 2. (a) Line traces taken approximately parallel to the grain boundaries in each material, after scaling to linearity in electron dose, and (b) now after scaling zero crystal thickness to unity. The approach used to choose regions of identical thickness in the two specimens is also illustrated.

quantitative analysis, regions of the images were digitised using an Eikonix densitometer at a resolution of 22 μm/pixel on the plates (0.18 nm/pixel on the specimens), and scaled to linearity in electron dose. The line traces shown in Fig. 2a, which correspond to strips that are approximately *parallel* to the grain boundaries, show a drop in intensity between the vacuum and the specimen edge which is caused by scattering out of the objective aperture by amorphous layers on the specimen surfaces. We assume here that the reduction in fringe contrast due to electrons that have been scattered by contamination but retained within the aperture is negligible, and the intensity at zero crystal thickness rather than the vacuum was accordingly scaled to unity for each data set, as shown in Fig. 2b. Three specimen thicknesses were chosen for analysis, corresponding to identical intensities of 0.7, 0.6 and 0.55 relative to the value of 1 at zero crystal thickness in each specimen. These regions have been marked in Figs. 1 and 2 using the symbols 1, 2 and 3, respectively. (This approach assumes that the grains in the two specimens scatter out of the objective aperture identically.) Thinner regions, at which amorphous layers on the specimen surfaces dominate the phase contrast, were avoided. The chosen regions were projected digitally over lengths of 19 nm parallel to the directions of the interfaces to produce one-dimensional profiles, each of which

was divided by a fitted background for comparison of the contrast with computer simulations. (A detailed account of the application of the Fresnel technique has been presented by Ross and Stobbs [1, 2], and will not be repeated here.)

Examples of regions of the experimental images and the corresponding intensity profiles are shown in the form of a montage in Fig. 3, and graphs of fringe contrast and spacing are plotted in Fig. 4 as a function of defocus. To first order, the ways in which the spacing and the contrast of the Fresnel fringes change with defocus can be used to determine the width and the "shape" of the boundary, respectively. It is clear that the spacings of the fringes in the two specimens are similar, and that there is a difference of almost exactly three in the magnitude of the Fresnel contrast, and hence in the value of ΔV, between the two specimens at all of the thicknesses examined.

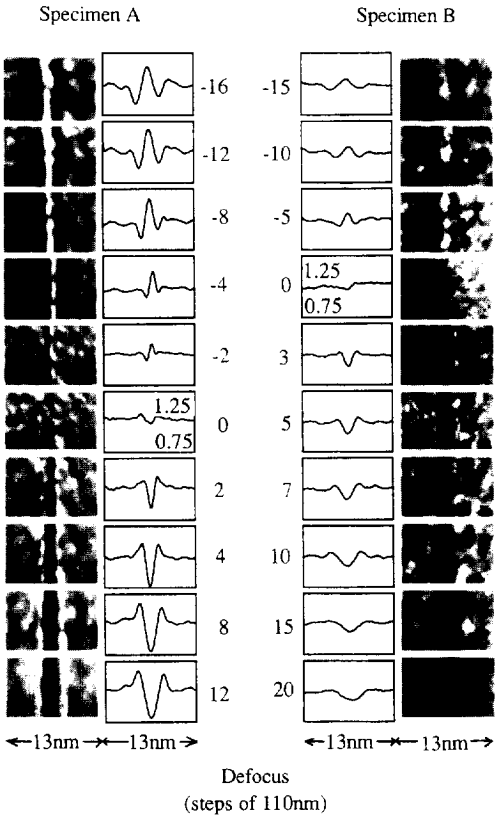

Fig. 3. Examples of the extracted regions and corresponding line profiles, for the middle of the three specimen thicknesses chosen for analysis.

Simulated Fresnel fringe profiles were generated using one-dimensional "continuum" (mean potential) multislice simulations [2]. A unit cell of (2048×1) pixels with a sampling density of 0.01 nm/pixel and a slice thickness of 0.1 nm was used. Values of 30 nm, 0.5 mrad. and 30 nm were used for the specimen thickness, beam convergence semi-angle and focal spread, respectively, and the sensitivity of the imaging behaviour to the form of the potential was investigated by changing the magnitude of the scattering potential difference ΔV, the width of the interlayer, and the form of the potential profile in the simulations. A value of V_0 for mullite was calculated using the neutral atom scattering factors of Rez et al. [5] (see below), and took a value of approximately 15.6 V over the entire mullite solid solution range. The best fits between the calculations and the experimental data, which are not shown here (for similar comparisons see e.g. Ref. [1]), were found to correspond to diffuse potential profiles (Gaussian profiles were fitted) with mean widths (full widths at half maximum) of 1.0 and 1.5 nm for specimens A and B, respectively. The fitted value of ΔV between the grain and the boundary was indeed three times higher for specimen A than for specimen B. Schematic diagrams of the best-fitting potential profiles for both specimens are shown in Fig. 5. The accuracy of the fitted parameters is estimated to be better than 10%.

While the potential profiles can be determined in this manner unambiguously, their interpretation requires considerable care. For example, large discrepancies, which are generally ascribed to the effects of bonding and specimen surface layers, have been found between electron holographic measurements of V_0 and calculations using neutral atom scattering factors [6]. The analysis presented below relies on the assumption that even if the absolute values of V_0 in the aluminosilicate system are affected by bonding, their relative values remain unchanged to first order. In this context, it should be noted that Fresnel contrast analysis is much more sensitive to local variations in the potential ΔV than to the absolute magnitude of V_0.

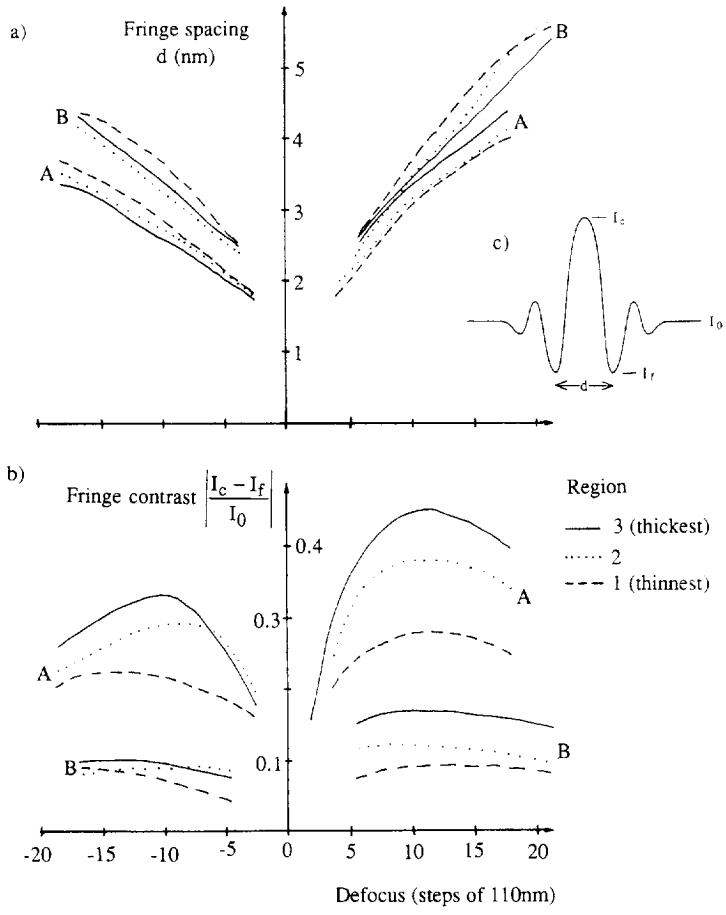

Fig. 4. Graphs showing the spacing and the magnitude of the experimental fringe contrast plotted as a function of defocus for specimens A and B. (c) shows the definitions of the symbols used.

The interpretation of the best-fitting potential profiles shown in Fig. 5 requires a knowledge of the nature of the elements whose concentrations are varying at the boundary. The approach taken below assumes that the compositions of the three-grain junctions and the grain boundaries in specimen A are identical, and makes use of energy dispersive X-ray spectroscopy (EDX) data for specimen A together with the Fresnel data to provide an accurate value for ΔV in specimen B.

4. Calibration of the Fresnel data

EDX spectra and linescans from specimens A and B were collected using a VG HB501 scanning transmission electron microscope (STEM) equipped with a windowless Link detector. As a result of the fine grain size in the specimens, it was not possible to locate and chemically analyse the specific boundaries that had been examined in the TEM; however, care was taken to ensure that the EDX work was carried out on typical grain boundaries for each specimen.

Examples of X-ray spectra from grains, grain boundaries and three-grain junctions are shown for both specimens in Fig. 6. When compared with the spectrum from the grain, there is a large rise in the Si signal relative to Al at both grain boundary and three-grain junction in specimen A, suggesting that the glassy material at the three-grain junction (and hence the grain boundary) has a composition which

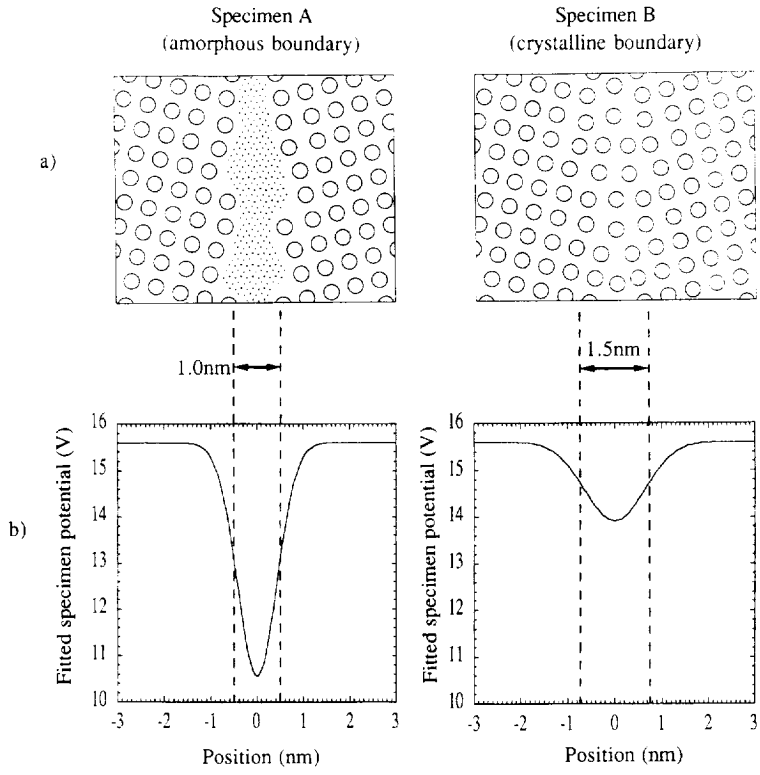

Fig. 5. (a) Schematic diagrams of the forms of the grain boundaries, alongside (b) the potential profiles determined from the Fresnel contrast data.

is rich in SiO_2. Qualitatively, the spectrum from the three-grain junction suggests an upper limit of $\sim 20\%$ Al in the glassy material (which is equivalent to 10 mol% Al_2O_3), although it is likely that some of the Al signal originates both from sputtered Al on the specimen surfaces caused by ion-beam thinning during specimen preparation and from surrounding areas of the specimen which have had electrons scattered back onto them from the microscope lens. (The Bremsstrahlung background will also be included in any chosen energy window). This is qualitatively in agreement with the composition of approximately 8 mol% Al_2O_3 which is predicted from the phase diagram of Klug et al. [7] for glass in equilibrium with mullite at 1600°C. In contrast, almost no difference in composition can be seen between the grain boundary and the grain in specimen B, indicating that the grain boundary observed in specimen B has a smaller Si concentration than that observed in specimen A as the two boundaries are known from the Fresnel data to have comparable widths[4]. Fig. 7 shows X-ray linescans obtained using energy windows centred on peaks corresponding to the presence of O, Al and Si, together with ratios of the linescans for O/Si, O/Al and Si/Al, which have been scaled to give the correct atomic ratios for stoichiometric mullite in the grains. (This removes the effects of the changes in specimen thickness which are visible in the original traces.) The three-grain junctions in specimen A show an O/Si ratio of almost exactly 2 and a Si/Al ratio which is greater than 5 (confirming

[4] Although the origin of the sulphur peak in the spectra from specimen B is not known, no difference in microstructure was seen between specimens of the same starting material as B which exhibited this peak and specimens which did not.

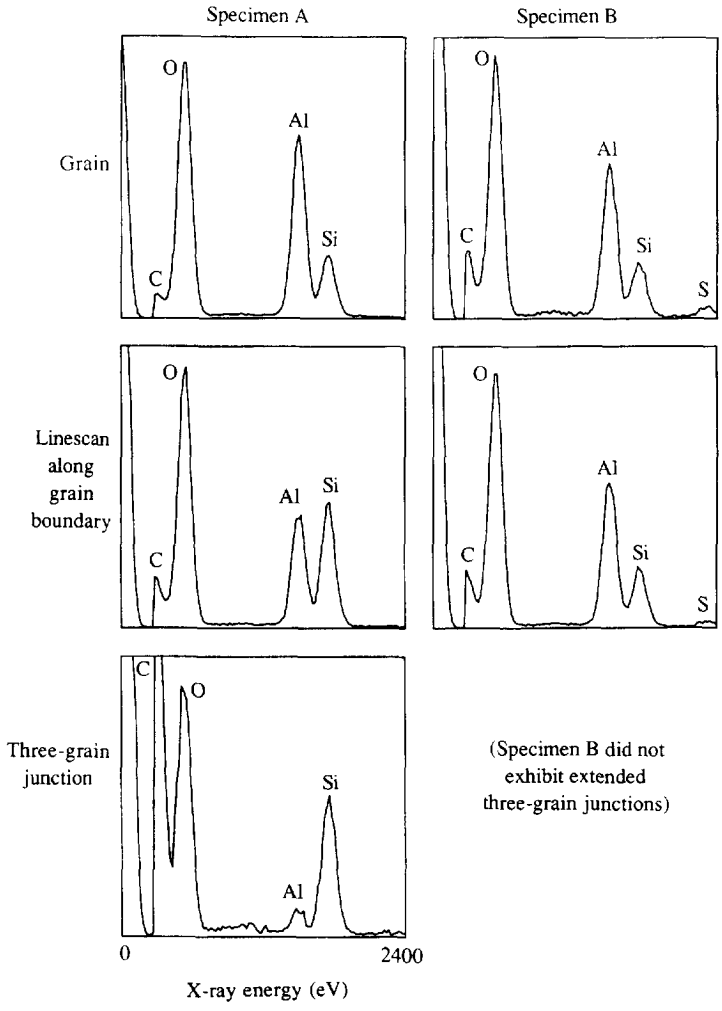

Fig. 6. STEM EDX traces from the areas in the two specimens indicated.

the upper limit of 10 mol% Al_2O_3 for the material at the boundary). No increase in the concentration of impurity elements at the grain boundary was seen. Although the same trends as for the three-grain junction are visible in a trace across a grain boundary in specimen A, the concentration changes are smaller as a result of the size and the broadening of the probe and slight misorientation of the boundary. Similar linescans across a grain boundary in specimen B show only noise. (It was not possible to obtain compositional information from extended three-grain junctions in specimen B.) Fig. 7 also shows a scan acquired from a grain without rastering the probe, from which it can be seen that errors due to electron-beam-induced loss of material are unlikely to alter the results significantly. Beam-induced mixing of species within the specimen is, however, more difficult to quantify.

The knowledge that specimen A has three-grain junctions and consequently grain boundaries that are rich in SiO_2 and contain not more than 10 mol% Al_2O_3, and that the grain boundaries in specimen B have a composition which is close to that of stoichiometric mullite, allows the Fresnel contrast data to be quantified. In particular, the scattering potential difference between the grain

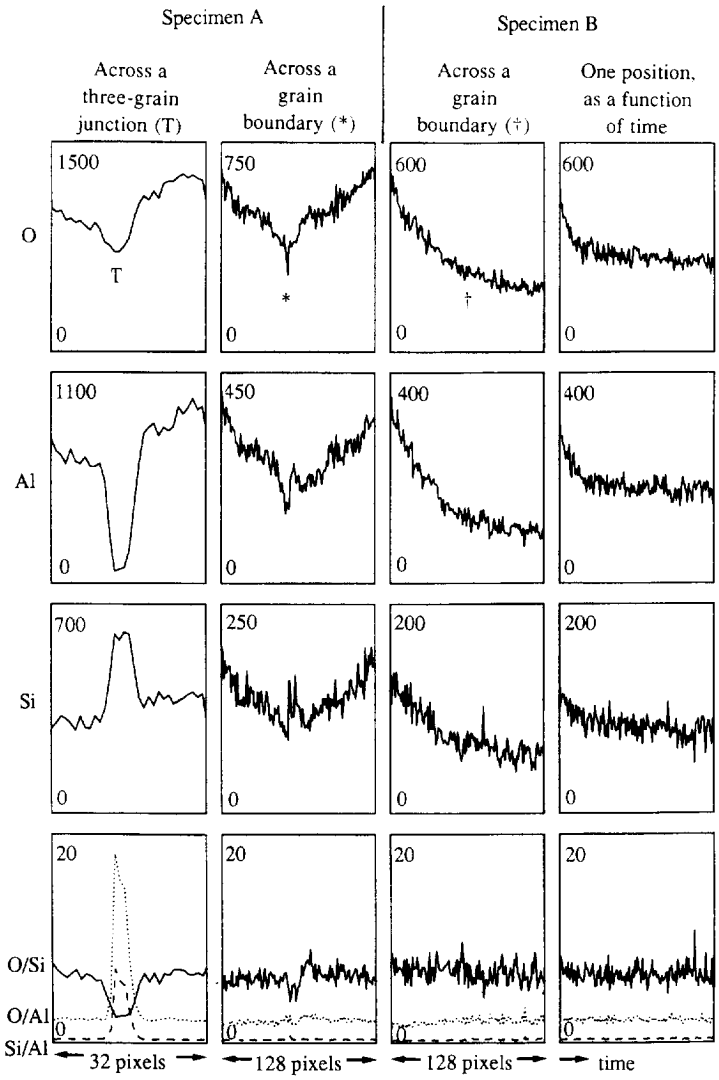

Fig. 7. STEM EDX linescans taken across the regions indicated for the two specimens. Ratios of spectra are also shown, with the values for the grains scaled to those for stoichiometric mullite.

and the grain boundary in specimen B can be calculated. As mentioned above, the mean potential V_0 in stoichiometric mullite is calculated to be 15.6 V if the neutral atom electron scattering factors[5] of Rez et al. [5] are used. Correspondingly, the presence of amorphous SiO_2 containing between 0 and 10 mol% Al_2O_3 implies that the boundaries in specimen A *must* have a value of V_0 (on the basis of their composition) of no less than 10.3 V and no more than 10.8 V (see Fig. 8). The grain boundaries in specimen B must therefore have a value of ΔV of $\frac{1}{3}$ times that for specimen A, and consequently V_0 and ΔV values of 13.8–14.0 V and 1.6–1.8 V, respectively. It is these values which must now be

[5] Mullite is expected to have between 50 and 60% ionic bonding [8]; however, the effects of ionicity are difficult to include in calculations. Here, it will be assumed that if neutral atom scattering factors are used consistently then *comparisons* of ΔV between compounds with different compositions are valid to first order.

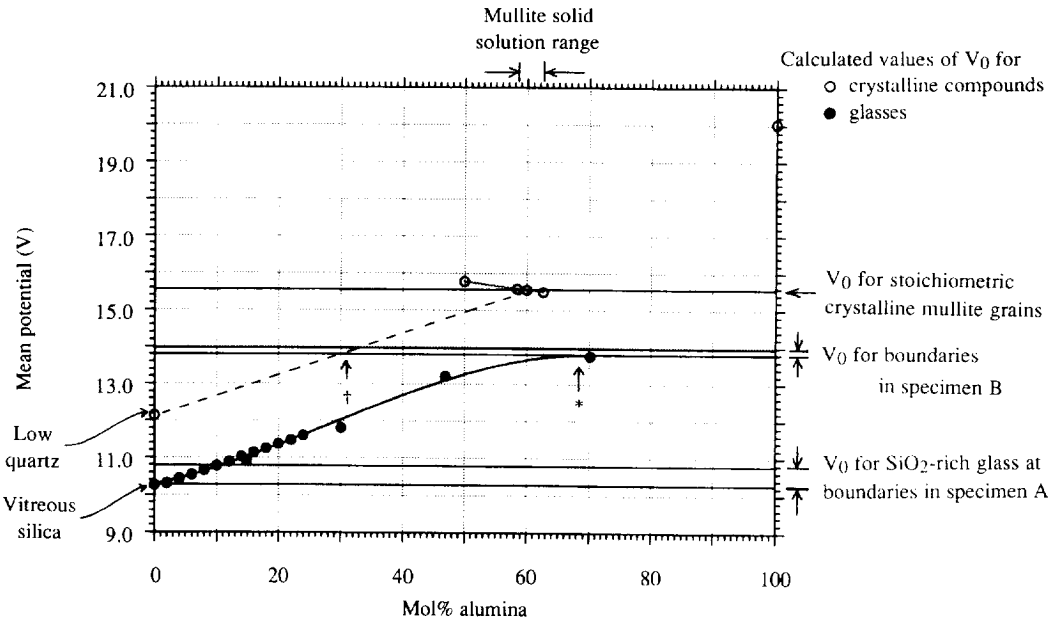

Fig. 8. Calculated and experimentally measured values of the average Coulomb electrostatic potential for the compositions indicated (see text for details). The solid and open circles represent glass and crystalline values respectively. * and † represent the compositions of glass and crystalline compounds which have the value of V_0 determined for the grain boundary in specimen B.

interpreted in terms of the possible composition and nature of the grain boundaries in specimen B.

5. Interpretation of the scattering potential difference in specimen B

An attempt to explain the observed contrast in specimen B in terms of a simple change in composition (i.e. *neutral* atom scattering factor) is illustrated in Fig. 8. Calculated values of V_0 for known crystalline and glass compounds in the aluminosilicate system are plotted as a function of composition, for comparison with the values of V_0 determined for the grain boundaries in the two specimens examined here. It is apparent from the V_0 values in the graph that, if the boundary in specimen B contained glass (though we know structurally that there is no evidence for the presence of a glassy phase), then it would have to have had an enrichment of Al_2O_3 (to a composition marked * in Fig. 8). However, this is in direct conflict with both the EDX analysis which showed a negligible change in concentration at the grain boundary and the diffuse dark field and high-resolution images which did not indicate that the boundary contained glass. For a crystalline boundary, if a linear relation could be assumed between the V_0 values of crystalline SiO_2 and stoichiometric mullite in Fig. 8, then the data would suggest the presence of a crystalline compound containing about 30 mol% Al_2O_3 at the boundaries in specimen B (marked † in Fig. 8). However, the values of V_0 for mullite and for a hypothetical crystalline compound containing 50 mol% Al_2O_3 (calculated using lattice parameters which had been extrapolated from those of lower silica mullite [9]) show that such a linear relation between V_0 and composition does not in fact exist, and no enrichment in Si was seen using EDX. This rather surprising result suggests that an alternative explanation for the experimentally measured contrast is required, and we accordingly consider the effects of changes in density, oxygen content, ionicity and space charge.

We first consider the possibility of changes in density or oxygen concentration at the grain

boundary in specimen B. Calculations using neutral atom scattering factors indicate that either a 10–12% reduction in density without a change in composition or a 30% decrease in oxygen content without a change in lattice parameter is required to reproduce the observed contrast at the boundary. The former explanation is unlikely both because such a lower-density crystalline compound does not exist in equilibrium and because changes in density at crystalline grain boundaries in ceramics are expected to be more localised than the 1.5 nm width of the observed potential profile.[6] Although oxygen vacancies are known to preferentially sink to grain boundaries, a 30% change in oxygen content also appears to be unreasonably high and no significant impurity segregation to the boundaries was observed using EDX. However, the fact that charged vacancies or solutes may be present at the grain boundary is an important point which will be discussed below.

The scattering factors f_{el} of the constituent atoms may themselves change if the ionic character of the material at the grain boundary differs from that in the grain. Rez et al. [5] have determined ionic scattering factors for certain isolated atoms. Assuming that the trends that they predict for the scattering factors $f_{el}(O^{2-}) \approx 2.1 f_{el}(O)$ and $f_{el}(Al^{3+}) \approx 0.11 f_{el}(Al)$ can be applied to mullite as a whole, calculations using these values indicate that the observed contrast at the grain boundary in specimen B would require approximately a 40–50% *increase* in the ionic character of the mullite at the grain boundary relative to that in the grain. This again appears to be unrealistically large a change, particularly in view of the fact that the mullite in the grain is predicted to have an ionicity of between 50% and 60% [8].

Now that we can discount all of the above effects as being of primary importance, we must consider carefully the effects of a space charge layer at the boundary in specimen B. This would be caused by a narrow distribution of charged vacancies or solute atoms at the grain boundary, and a wider layer of charge of the opposite sign (usually as free carriers) to ensure overall charge neutrality within the material [10]. Schematic diagrams of the possible forms of such a space-charge layer are shown in Fig. 9. Only the simplest models to describe a space-charge layer are considered here, in order to gain a preliminary understanding of their contribution to V_0. Dunin-Borkowski et al. [11] have considered the magnitudes and the widths of the potential profiles which are associated with space-charge layers at interfaces. The relevant equations are summarised in Table 1 for wider and narrower charge distributions that have full widths at half maximum d_f and d_b, respectively. Expressions are given for both Gaussian and exponential charge distributions, which can be regarded as extreme limits for the forms the charge distributions could take up at a grain boundary[7]. Using a value of 6 for the dielectric constant of mullite, the calculations of Dunin-Borkowski et al. [11] allow the magnitude and the width of the free charge distribution required to reproduce the full potential difference observed for the crystalline boundary B to be determined. For a narrower charge distribution with a width of 0.1 nm, if Gaussian charge distributions are assumed the free charge required corresponds to a sheet number density of $1 \times 10^{18}\ m^{-2}$ with a full width at half maximum of 3.4 nm. The equivalent figures for exponential distributions are $2 \times 10^{18}\ m^{-2}$ and 1.4 nm. The *sense* of the observed contrast is consistent with the presence of a narrow layer of negative charge at the boundary and a wider distribution of positive charge. The fitted profiles,[8] which reproduce both the magnitude and

[6] Given that we are confident that we are dealing with a crystalline boundary, the local rigid-body displacement (giving a reduction in density and thus V_0) will undoubtedly affect the Fresnel contrast. We will return to this point once we have clarified the primary origin of the contrast seen which, on the basis of the contrast width, cannot be the rigid-body displacement.

[7] The exponential dependence which is predicted for the decrease of the defect or solute charge density with distance from an interface was originally formulated for space charge layers at free surfaces and relies on the presence of an infinite source of charged defects at the boundary [12]. This condition may not always be satisfied. For example, a Gaussian distribution is more representative of both an impurity *diffusion* profile and the form of a ground-state free carrier wave function [13].

[8] An increase in the width of the narrower charge distribution, which was here assumed to be confined to 0.1 nm, would require a larger charge density to fit the observed contrast.

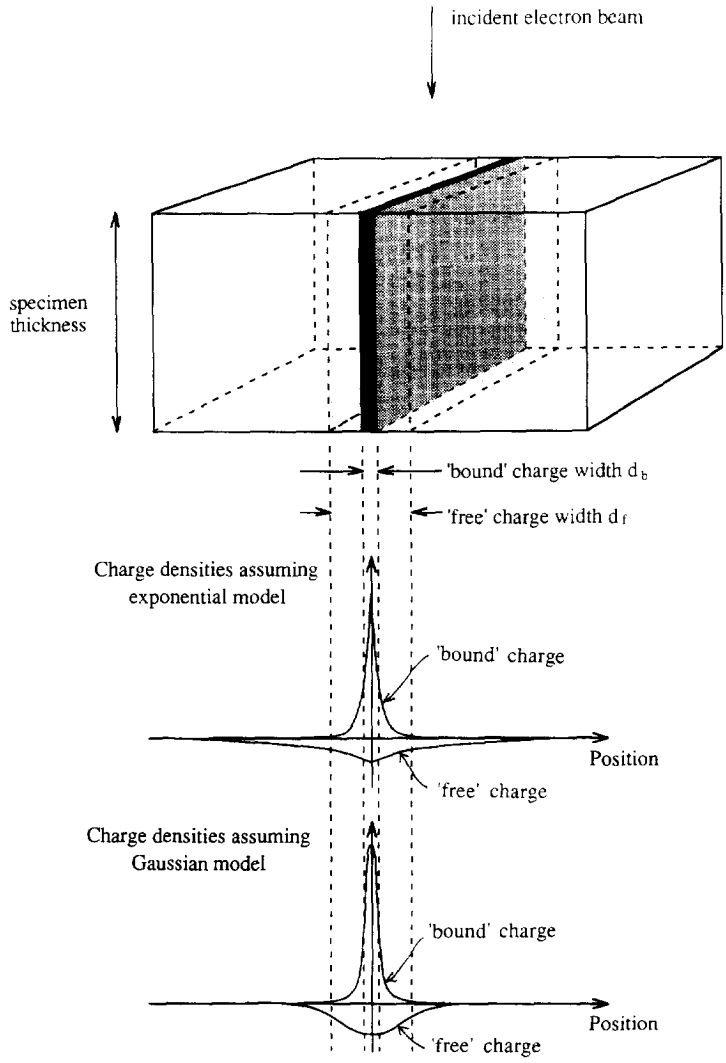

Fig. 9. Schematic diagram showing the typical geometry of a cross-sectional TEM specimen containing a space-charge layer at a grain boundary, and the forms of possible exponential and Gaussian charge distributions.

the width of the experimentally determined potential profile at the grain boundary in specimen B, are summarised in Table 2 and are shown in Fig. 10. While the large difference between the magnitudes and the widths of the charge distributions which are inferred using Gaussian and exponential model charge distributions should be noted, it is significant that charge distributions of this magnitude have been reported in other ceramics, see e.g. Ref. [14]. It is also interesting that Ravikumar et al. [15] have used electron holography to determine that a Mn-doped grain boundary in $SrTiO_3$ also contained a negative boundary charge, a wider positive charge and a potential profile of width approximately 1.5 nm.

Although the evidence that has been presented for the presence of a space-charge layer is not unequivocal as a result of possible errors in calculated values of V_0, we have shown that the width of the Fresnel contrast observed *is* consistent with a dominant contribution due to space charge. The number density of charged solute atoms or vacancies

Table 1
Calculated contribution to the scattering potential at a space-charge layer in an isotropic material, from the work of Dunin-Borkowski et al. [11]

Form of charge distributions at grain boundary	Electrostatic contribution to the magnitude of the potential at the grain boundary	Full width at half maximum of potential, as a least-squares biquadratic fit to the true relation (an analytical solution is not possible)
Gaussian	$3.0656\times10^{-9}\left(\frac{N_{2D}}{\varepsilon_r}\right)(d_f-d_b)$	$1.06\times10^{-12}+0.592d_b+0.424d_f+9.56\times10^{6}d_bd_f-9.64\times10^{6}d_b^2-1.56\times10^{6}d_f^2$ (accurate to better than 2.4% for $0\leqslant d_b<d_f\leqslant10^{-8}$ m)
Exponential	$6.5264\times10^{-9}\left(\frac{N_{2D}}{\varepsilon_r}\right)(d_f-d_b)$	$3.92\times10^{-12}+1.43d_b+1.03d_f+3.18\times10^{7}d_bd_f-3.19\times10^{7}d_b^2-5.28\times10^{6}d_f^2$ (accurate to better than 2.0% for $0\leqslant d_b<d_f\leqslant10^{-8}$ m)

d_b and d_f are the full widths at half maximum of the narrower and wider charge distributions, respectively, N_{2D} is the total projected positive or negative charge number density in each charge distribution, and ε_r is a dielectric constant. SI units have been used throughout.

Table 2
Best-fitting values of N_{2D} and d_f to the experimental data for specimen B

Form of charge distributions	N_{2D} (m^{-2})	d_f (nm)
Gaussian	1×10^{18}	3.4
Exponential	2×10^{18}	1.4

In these calculations, it is assumed that the space-charge layer accounts for the total magnitude of ΔV, and that d_b and ε_r take values of 0.1 nm and 6, respectively.

which has been inferred is necessarily associated with a local change in bonding character at the boundary. The approach to the calculation that we have taken is to a degree equivalent to considering a change in the local ionicity, so that the only further effect we need to consider in assessing the full origin of the change in potential at the boundary is that due to the reduction in density associated with the geometric form of the grain boundary. If we assume an exponential form for the charge distributions [12], although there is necessarily a systematic error in the magnitude of the fitted space charge resulting directly from the effects of a reduction in density at the boundary, we are still confident that the fitted boundary charge density is not in error by more than $\pm$ 10% as changes in the form of the Fresnel scattering behaviour (due to reductions in density at the boundary) would have been apparent.

6. Conclusions

Grain boundaries in two mullite specimens have been characterised using Fresnel contrast analysis and energy dispersive X-ray spectroscopy. A relative comparison of the magnitude of the Fresnel contrast at a boundary in each specimen, together with chemical characterisation of a glassy interfacial compound in one specimen using EDX, have allowed the absolute magnitude of ΔV for the second, crystalline grain boundary to be determined without the need for a knowledge of the specimen thicknesses examined and without the need to consider the effects of inelastic scattering. The interpretation of this value of ΔV has shown that the contrast cannot be explained solely by a change in composition, density or ionicity, but is consistent with a dominant contribution associated with the presence of a space-charge layer consisting of a localised distribution of positive charge and a wider distribution of negative charge, with projected electrically active concentrations which are of the order of 10^{18} m^{-2}. It is hoped that the Fresnel contrast approach illustrated here will be developed for the characterisation of charged layers at interfaces in a wide variety of systems.

Acknowledgements

We wish to thank the Education Ministry of Turkey and the E.P.S.R.C. for financial support.

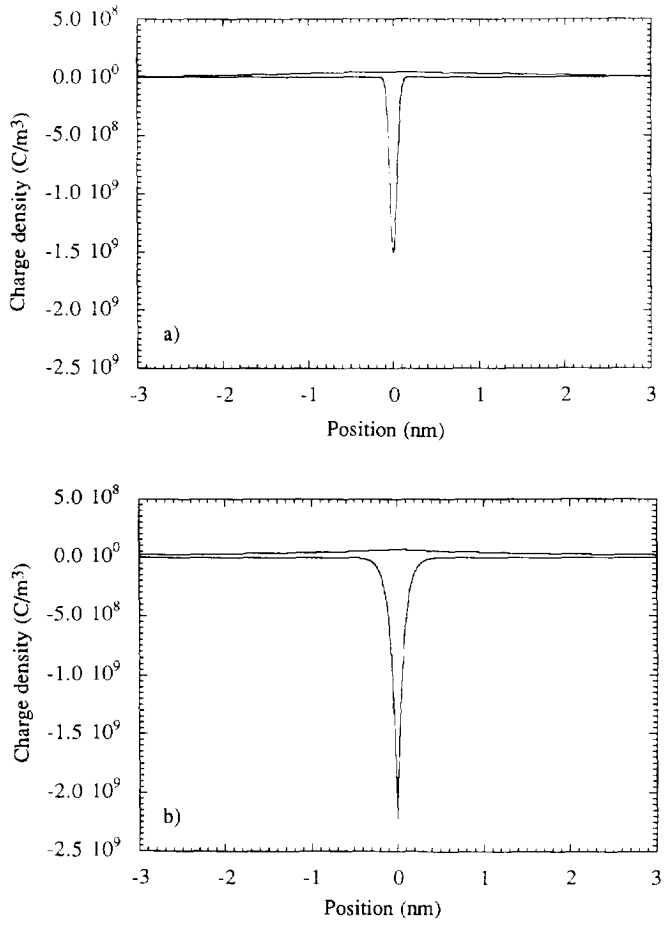

Fig. 10. The best-fitting (a) Gaussian and (b) exponential charge distributions to the fitted potential profile for specimen B, assuming that space charge accounts for the total measured change in potential.

References

[1] F.M. Ross and W.M. Stobbs, Phil. Mag. A 63 (1991) 1.
[2] F.M. Ross and W.M. Stobbs, Phil. Mag. A 63 (1991) 37.
[3] J.N. Ness, W.M. Stobbs and T.F. Page, Phil. Mag. A 54 (1986) 679.
[4] F. Kara, Ph.D. Thesis, University of Cambridge, 1994.
[5] D. Rez, P. Rez and I.P. Grant, Acta Crystallogr. A 50 (1994) 481.
[6] M. Gajdardziska-Josifovska, M.R. McCartney, W.J. de Ruijter, D.J. Smith, J.K. Weiss and J.M. Zuo, Ultramicroscopy 50 (1993) 285.
[7] F.J. Klug, S. Prochazka and R.H. Doremus, J. Am. Ceram. Soc. 70 (1987) 750.
[8] R.W. Davidge, Mechanical Behaviour of Ceramics (Cambridge University Press, Cambridge, 1977).
[9] W.E. Cameron, Am. Mineral. 62 (1977) 747.
[10] K.L. Kliewer and J.S. Koehler, Phys. Rev. 140 (1965) A1226.
[11] R.E. Dunin-Borkowski, W.O. Saxton and W.M. Stobbs, Acta Crystallogr. A 52 (1996) 705.
[12] J. Frenkel, Kinetic Theory of Liquids (Oxford University Press, New York, 1946).
[13] E.F. Schubert, Doping in III–V Semiconductors (Cambridge University Press, Cambridge, 1993).
[14] J.A.S. Ikeda and Y.-M. Chiang, J. Am. Ceram. Soc. 76 (1993) 2437.
[15] V. Ravikumar, R.P. Rodrigues and V.P. Dravid, J. Phys. D 29 (1996) 1799.